Optimization of Geometric Nozzle Parameters for Chocolate-Based 3D Printing

MAE 4530 / 5530: Computer-Aided Engineering for Biological Systems

May 6th, 2026

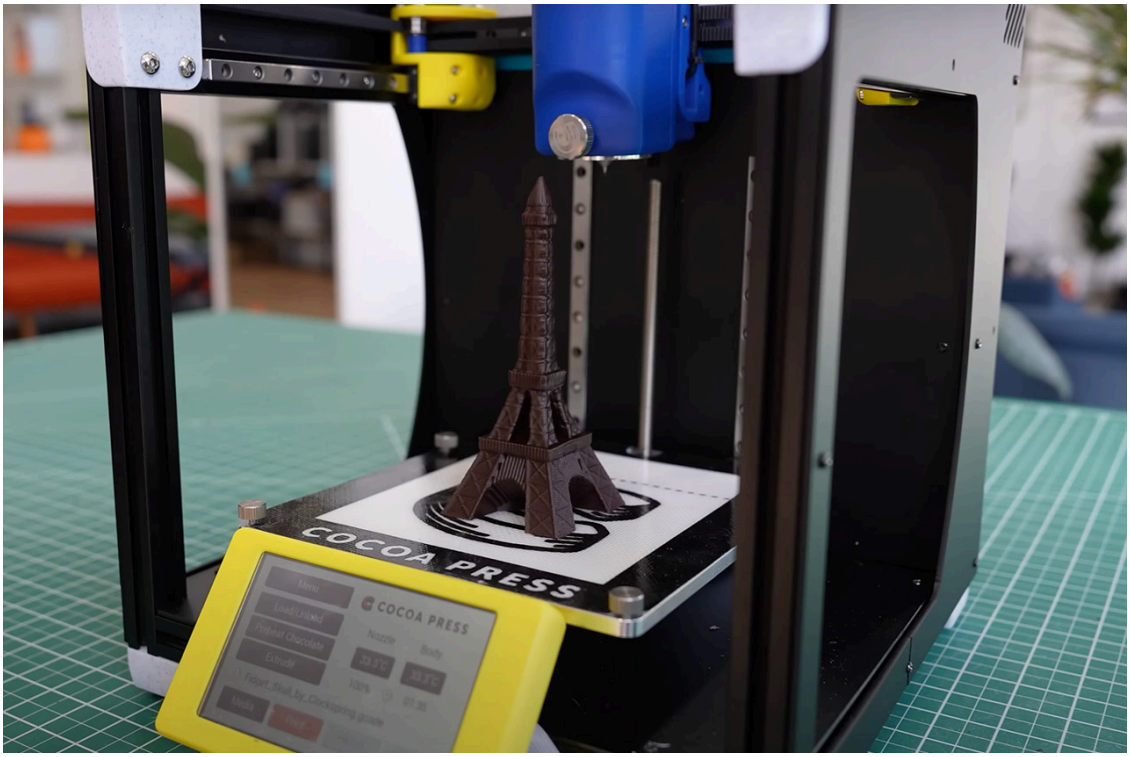

Contributors:

© Andrew D’Onofrio, Joanna Tan, Mary Conlan

Table of Contents

1.0 EXECUTIVE SUMMARY

Our team optimizes the nozzle geometry for popular commercial chocolate 3D printers (i.e. Cocoa Press 1 3D Printer) to improve structural performance and aesthetics of chocolate. The Cocoa Press 3D-Printer is a standard FDM (Fused Deposition Model) 3D-printer, integrating a heated nozzle to layer cross-sections of liquid filament and create a three-dimensional design. Given the novel method for pre-heating the chocolate in a reservoir prior to deposition, these designs bypass typical tempering recommendations for commercial chocolate figures. This limits structural strength through reduced internal crystalline structures formed by sugar, forming a softer and more deformed final product. Our team analyzes methods for optimizing the Cocoa Press 1 3D-Printer nozzle geometry to refine outlet temperature and tempering across different input parameters (feed rate, cocoa percentage, etc.). This is accomplished by iterating across several nozzle diameters and lengths to isolate the temperature profile of liquid chocolate fed through a commercial nozzle. Through finite-element analysis (FEA) in COMSOL, none of the tested nozzle geometries were found to achieve effective chocolate tempering under the simulated operating conditions. Across all configurations, outlet temperatures remained nearly constant, indicating insufficient thermal regulation within the nozzle to induce the phase transformations required for proper tempering. While variations in nozzle diameter and length influenced flow behavior, particularly peak velocity and flow development, neither produced meaningful changes in outlet temperature from the baseline of 322 K. As a result, the Cocoa Press system in its current form does not achieve tempering through geometric modification alone. These findings suggest that additional process controls, such as active cooling or upstream tempering mechanisms, are necessary to achieve structurally stable and properly crystallized chocolate during extrusion.

Key Words: Chocolate Rheology; 3D Food Printing; 3D-Printer Nozzles; Cocoa Press 1; Tempering

2.0 INTRODUCTION

Chocolate-based 3D printing is a recent, novel approach for creating chocolate designs, and tempering large chocolate designs is an essential materials-processing problem in chocolate 3D printing. With the lack of proper tempering during extrusion, it directly limits structural integrity, surface quality, and commercial viability. Proper tempering forms stable cocoa butter crystals which give chocolate its strength, gloss, snap, and resistance to deformation [1]. Without controlled crystallization, printed parts become softer, warp more easily, lose fine detail, and have reduced shelf stability. This limits both the aesthetic quality and mechanical performance [1]. Optimizing nozzle geometry is critical towards the advance of chocolate 3D printing since it directly influences the outcome of the chocolate once it cools. For this specific reason, our research directly aims to improve production quality and viability of chocolate produced by on-market, commercial chocolate 3D printers.

Additionally, our work bridges together food science, heat transfer, additive manufacturing, and design, where the underlying engineering principles extend far beyond confectionery applications. These same principles apply to bioprinting hydrogels, pharmaceutical melt extrusion, soft polymer manufacturing, and functional food fabrication. This process is generally applicable where precise thermal regulation determines structural integrity, mechanical performance, and material stability. By optimizing nozzle geometry to influence solidification and crystallization in real time, this research contributes to a broader understanding of phase-controlled additive manufacturing, with potential impact in bioprinting, personalized nutrition, and sustainable materials processing.

3.0 PROBLEM STATEMENT AND DESIGN OBJECTIVES

A chocolate-specific 3D printer follows a similar design to a Direct Ink Writing (DIW) printer and a Fused Deposition Modelling (FDM). Although chocolate 3D printing has some minor process modifications to account for the unique viscosity of chocolate in comparison to traditional thermoplastics, all methods involve layered printing of objects on a heated bed. More specifically, these printers use solid logs of chocolate that are melted in a chamber above the nozzle as the extrusion material. Melted chocolate is fed through the nozzle via a motor-driven plunger, then extruded out of the nozzle tip. There are heating elements along the chamber, to keep the chocolate at the optimal extrusion temperature (~33°C, 306 K) as it passes through the cartridge. The chocolate is then pushed out of a nozzle, building layer by layer of chocolate. Convection inside the fluid occurs as the chocolate moves through the nozzle due to the pressure-driven flow created by the plunger. As it cools through the nozzle, the viscosity increases in both the radial and axial directions, effectively thickening as it gets closer to the exit point. Conduction takes place between the molten chocolate and the stainless-steel nozzle walls as heat transfers through the metal.

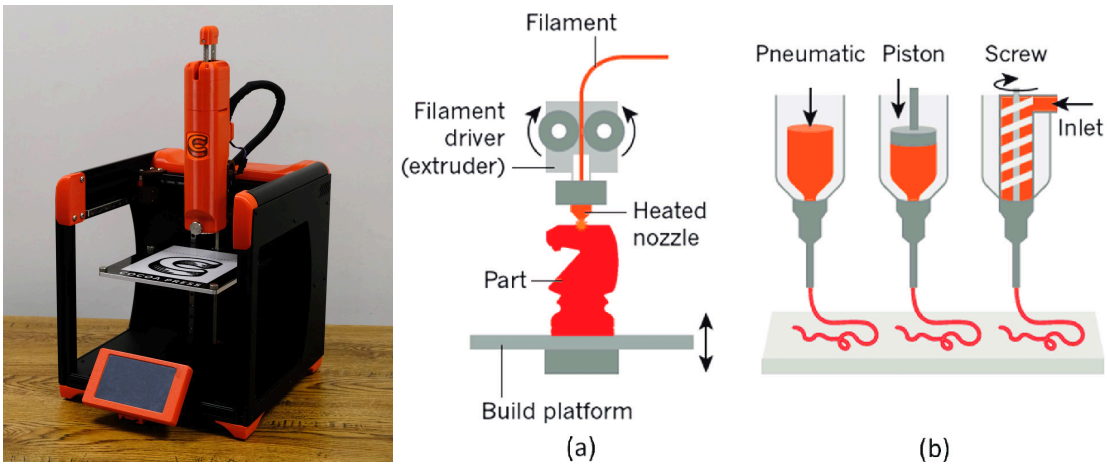

Figures 3.1 & 3.2: The commercially available Cocoa Press 1 3D-Printer [2], and methods for extrusion based printing such as Fused Deposition Modelling (FDM) (a) and Direct Ink Writing (DIW) (b).

3.1 Problem Statement

Chocolate is highly sensitive to temperature, and its mechanical and visual properties depend strongly on a process known as tempering. Tempering involves carefully controlling the melting, cooling, and reheating of chocolate to stabilize specific cocoa butter crystal structures. Tempering is important for creating chocolate design, specifically 3D printing, as the technique allows for stronger, more durable results. Tempered chocolate also has a glossy finish and an aesthetically pleasing facade. Most

commercially available chocolate 3D printers, including systems such as the Cocoa Press, do not explicitly advertise that their machines temper chocolate during the printing process. Instead, they typically rely on pre-tempered chocolate, meaning the chocolate has already undergone the tempering process before being loaded into the printer. The printer then maintains the chocolate within a narrow temperature range that allows it to remain extrudable while attempting to preserve the existing crystal structure. It is important to know if the chocolate is tempered properly, if at all, when used for specific applications. This project will iterate through possible nozzle diameters and chamber lengths to determine whether it is all possible to 3D print tempered chocolate, and whether any commercially available designs from Cocoa Press temper already.

3.2 Research/Design Objectives

The primary objective of this study is to evaluate whether a chocolate extrusion nozzle can maintain a proper temperature range that supports tempering during layer-by-layer deposition. Multiphysics modeling in COMSOL will be used to analyze coupled heat transfer and fluid flow within the cartridge, stainless-steel nozzle, and surrounding environment.

The specific objectives are as follows:

1. Simulate heat transfer within the molten chocolate and nozzle assembly to determine axial and radial temperature distributions during extrusion.
2. Investigate the influence of convection and conduction on cooling behavior as the fluid approaches the nozzle tip.
3. Evaluate the effect of nozzle geometry, specifically diameter and length, on thermal exposure, and overall temperature uniformity.
4. Compare alternative design configurations to identify conditions that optimize the chance of achieving tempered chocolate when extruded to improve its strength.
5. Prove existing technology on the market achieves conditions required for tempering, or recommend new geometric configurations that satisfy the constraints.

These design objectives help to establish measurable criteria for assessing the feasibility of tempering with commercially available chocolate 3D printing systems.

4.0 METHODS

Nozzle-based extrusion of non-newtonian fluids from a 3D-printer involves a combination of creeping fluid flow and heat transfer with multiple materials. In practice, these extrusion mechanisms are optimized by concentrating on the printer hot-end, more specifically the stainless-steel nozzle. By simplifying heating and cooling effects from the barrel heater and atmospheric cooling as boundary conditions with constant behavior, the model can be simplified as an axisymmetric model of the nozzle cross-section with flowing, fluid chocolate. This requires a steady-state, coupled "Fluid Flow" model and "Heat Transfer in Fluids" model in the COMSOL software for demonstrating the thermal and flow conditions for the system.

4.1 Schematic and Qualitative Description of the Physics

The following diagram (Figure 4.1 & 4.2) illustrates the physical behavior of the chocolate extrusion process. In this system, liquid chocolate flows through the stainless steel nozzle of the Cocoa Press 1 3D printer while experiencing both fluid flow and heat transfer. The chocolate enters the nozzle at a preset temperature and moves toward the outlet as it is deposited during printing. As the chocolate travels through the nozzle, heat is transferred between the chocolate and the surrounding stainless steel walls through conduction, cooling the chocolate, while additional heat may be lost to the surrounding environment. The outlet temperature is an important factor because it influences whether the chocolate remains within a temperature range suitable for tempering. From a fluid flow perspective, the chocolate moves slowly through the narrow nozzle and behaves as a highly viscous fluid, resulting in creeping flow conditions (Re << 1). The chocolate interacts with the nozzle walls through a no-slip boundary condition, meaning the fluid velocity at the wall surface is essentially zero, and it exits the nozzle into the atmosphere at approximately ambient pressure. Additional details of the physical setup are shown in the "Overview of Basic Schematic," where the two main components of the liquid chocolate and the nozzle are illustrated separately for clarity.

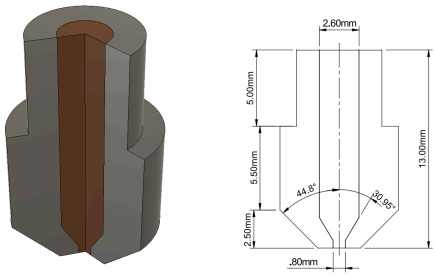

Figure 4.1 & 4.2: Simplified design of the stainless-steel nozzle implemented in typical extruder-based printing with example input geometric dimensions completed in Fusion360 software.

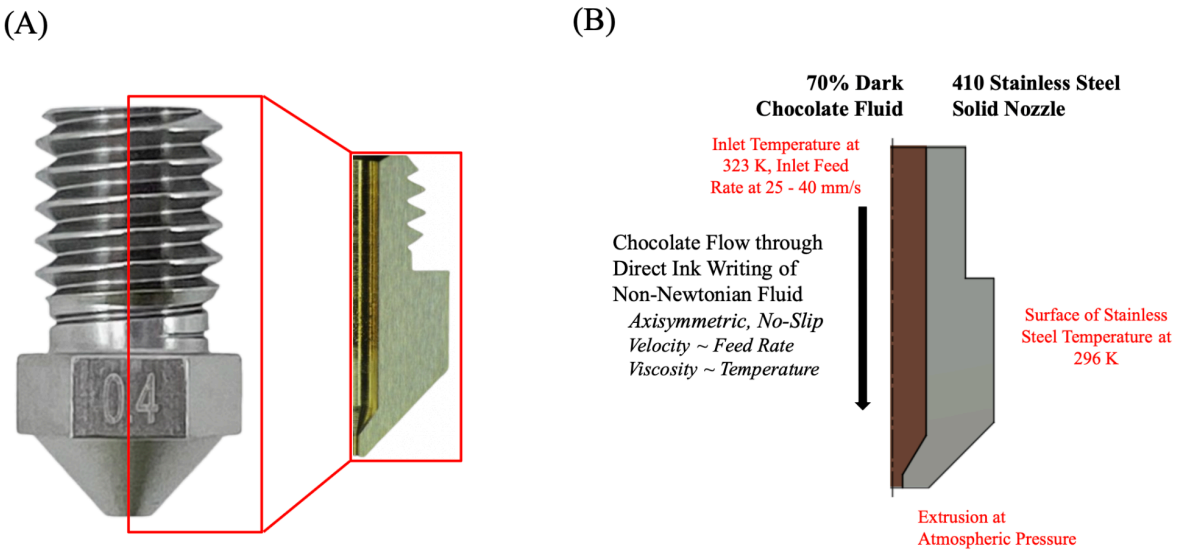

Figure 4.3: Physical geometry referenced for the simplified schematic (A), and a qualitative schematic of the chocolate extrusion through nozzle (B).

4.2 Assumptions

1. **Axisymmetric Model:** With rotational symmetry, the model is simplified as a cross-sectional portion of the nozzle and fluid domain. This reduces computational complexity while still capturing the main heat transfer and flow behavior within the extrusion system.
2. **Creeping Flow (Laminar Flow):** Considering the short flow distance and low feed rate (low velocity), the chocolate flow is modeled as laminar or creeping flow, where viscous forces dominate and inertial effects are negligible.
3. **Steady-State Flow & Heat Transfer:** Although time-dependent simulations are possible, the analysis focuses on steady-state conditions. The startup heating phase and the ending phase of printing are not considered because most of the printing process occurs only when steady-state conditions are reached.
4. **Single Phase, Uniform Proportion of Elements:** Chocolate is treated as a homogeneous mixture. The model assumes cocoa solids, cocoa butter, and sugar are evenly distributed throughout the fluid and remain in a consistent liquid phase during extrusion.
5. **Incompressible Flow:** The fluid is assumed to be incompressible because extrusion occurs at very low Mach numbers, meaning density changes in the chocolate are negligible.

6. **No-Slip Wall Boundary:** A no-slip boundary condition is applied at the nozzle walls, meaning the chocolate velocity at the wall surface is assumed to be zero. This is a standard assumption for viscous flow inside pipes and channels.
7. **Non-Newtonian Viscosity Model (Cross–WLF Model):** Chocolate exhibits non-Newtonian behavior, so the viscosity is modeled using the Cross–WLF model. This model captures both shear-thinning behavior and the strong dependence of viscosity on temperature. It combines the Cross model for shear rate effects with the Williams–Landel–Ferry (WLF) equation to account for temperature variations, allowing for a more accurate representation of molten chocolate as it flows and cools through the nozzle. This model is almost exclusively used for modeling FDM applications, so the extrapolation to chocolate FDM is valid.
8. **Controlled Environment Assumption:** Environmental factors such as humidity, air saturation, and external heat exposure are not included in the model. The printer is assumed to operate in a controlled environment so the study can focus specifically on the thermal behavior inside the nozzle.
9. **Stable Heater Temperature:** The cartridge heater is assumed to maintain a stable temperature using a standard PID control system. While real systems may experience small temperature fluctuations depending on the printer assembly, the model approximates a constant heating condition.
10. **Model Scope Limitation:** The simulation focuses on predicting temperature distribution and outlet temperature under steady operating conditions using manufacturer-provided parameters and documented operating conditions.

4.3 Governing Equations

Cylindrical, axisymmetric governing equations are needed to describe the behavior of the fluid as affected by heat and fluid velocity. This model utilizes a simplified form of the Navier-Stokes equation to model the fluid, as well as the heat transfer equation to describe both the heat transfer in the die and the fluid. Both equations provide outputs in terms of radial and axial (no theta-dependence).

Equation #1: Momentum Conservation Equation for Fluid-Flow

$$0 = -\frac{\partial p}{\partial z} + \eta\left(\frac{1}{r}\frac{\partial}{\partial r}\left(r\frac{\partial u_z}{\partial r}\right) + \frac{\partial^2 u_z}{\partial z^2}\right) \quad [1]$$

$$-\frac{\partial p}{\partial z}\ represents\ axial\ pressure\ gradient$$

$$\frac{1}{r}\frac{\partial}{\partial r}\left(r\frac{\partial u_z}{\partial r}\right)\ represents\ radial\ diffusion\ of\ momentum$$

$$\frac{\partial^2 u_z}{\partial z^2}\ represents\ axial\ diffusion\ of\ momentum$$

There will be no transient velocity term, (i.e. the nozzle is in steady state throughout) and that the model is at creeping flow which cancels the inertial term. The viscosity term is temperature-dependent through the Cross-WLF Model and is represented with a function relative to the geometry in the nozzle.

Equation #2: Energy Conservation Equation for Heat Transfer

$$Fluid\ Chocolate:\ \rho_{choc} c_{p,choc}\left(u_r\frac{\partial T}{\partial r} + u_z\frac{\partial T}{\partial z}\right) = k_{choc}\left(\frac{1}{r}\frac{\partial}{\partial r}\left(r\frac{\partial T}{\partial r}\right) + \frac{\partial^2 T}{\partial z^2}\right) + \tau : \nabla u \quad [2]$$

$$Stainless\ Steel\ Nozzle:\ \rho_{steel} c_{p,\,steel}\left(u_r\frac{\partial T}{\partial r} + u_z\frac{\partial T}{\partial z}\right) = k_{st.}\left(\frac{1}{r}\frac{\partial}{\partial r}\left(r\frac{\partial T}{\partial r}\right) + \frac{\partial^2 T}{\partial z^2}\right) \quad [3]$$

$$\tau : \nabla u\ represents\ viscous\ dissipation$$

$$\rho c_p\left(u_r\frac{\partial T}{\partial r} + u_z\frac{\partial T}{\partial z}\right)\ represents\ radial\ and\ axial\ convection$$

$$k\left(\frac{1}{r}\frac{\partial}{\partial r}\left(r\frac{\partial T}{\partial r}\right) + \frac{\partial^2 T}{\partial z^2}\right)\ represents\ radial\ and\ axial\ conduction$$

The energy conservation equation determines the heat transfer for both the fluid chocolate and the stainless steel nozzle. The flow is a steady state scenario with no transient terms for heat transfer. Additionally, considering the fluid flow and external airflow across the nozzle, both energy conservation equations include conduction and convection in the system. Finally, there are no external heat generation or source terms present in either fluid or chamber.

4.4 Boundary Conditions and Geometry

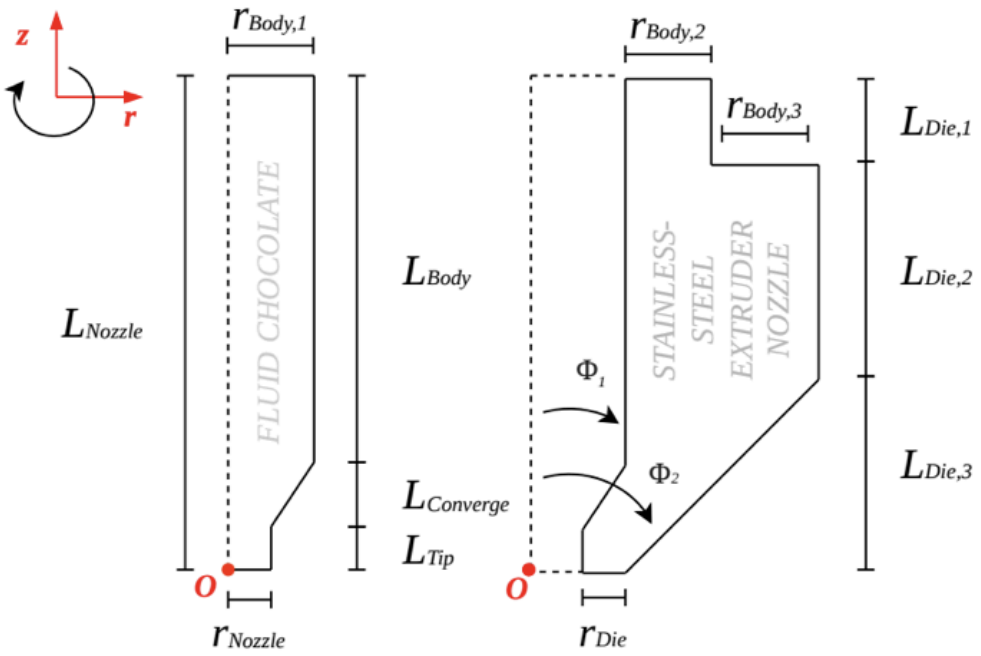

Figure 4.4: Detailed schematic of the nozzle geometry for the given COMSOL model.

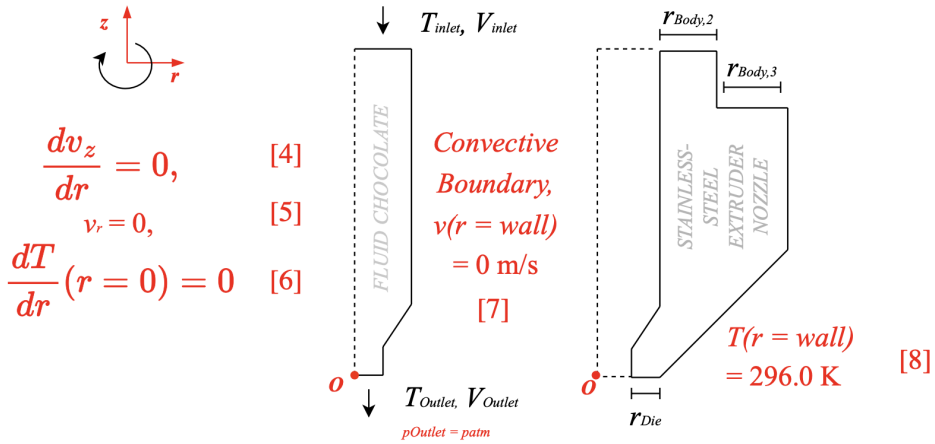

Figure 4.5: Detailed schematic of the nozzle boundary conditions for the given COMSOL model.

4.4.1 Input Parameters

Variable	Variable Description	Value	Units	Source Citation
$c_{p,choc}$	Specific Heat of Chocolate	2100	J/kg·K	[3]
$c_{p,steel}$	Specific Heat of Stainless Steel	500	J/kg·K	[4]
$F_{plunger}$	Estimated Plunger Force	45	N	[5]
$h_{st.,\,air.}$	Thermal Convection on the Stainless Steel with Forced Air	8.65	W/m^2·K	See Appendix A
$k_{st.}$	Thermal Conductivity of Stainless Steel	14.9	W/m·K	[6]
η	Chocolate Viscosity	*Reference Model*	Pa·s	See Appendix B
η_0	Zero-Shear Chocolate Viscosity	*Reference Model*	Pa·s	See Appendix B
p_{atm}	Outlet Pressure	101325	Pa	Atmospheric Standard
ρ_{choc}	Density of Chocolate	1229	kg/m^3	[7]
ρ_{steel}	Density of Stainless Steel	7750	kg/m^3	[4]
τ_y	Yield Stress	*Reference Model*	Pa	See Appendix B
T_{amb}	Ambient Temperature	296	K	Room Temperature Standard
T_{in}	Input Temperature	323	K	[8]
v_{in}	Feed Rate Velocity	25.0	mm/s	See Appendix C

Fluid Geometry: $\phi_1 = 61.9°$ $r_{Nozzle} = 0.4\ mm\ (Ind.\ Variable)$ $r_{Body,1} = 1.3\ mm$ $L_{Tip} = 0.5\ mm$ $L_{Converge} = 1.5\ mm$ $L_{Body} = 11.0\ mm$ **Nozzle Geometry:** $\phi_2 = 89.6°$ $r_{Die} = 1.0\ mm$ $r_{Body,1} = 1.5\ mm$ $r_{Body,2} = 1.03\ mm$ $L_{Die,1} = 5.0\ mm$ $L_{Die,2} = 5.5\ mm$ $L_{Die,3} = 2.5\ mm$	**Fluid Flow Characteristics:** $Re << 1\ (Creeping\ Flow)$ $p_{atm} = 1\ atm\ (101325\ Pa)$ $v_{in} = 25\ \frac{mm}{s}\ (Ind.\ Variable)$ **Fluid Flow Properties** ***See Appendix B*** **Heat Transfer Properties:** $T_{In} = 27\ °C$ $T_{Inf.} = 23\ °C$ $T_{Out} = T_{Tg}\ (Dep.\ Variable)$ $k_{St.} = \frac{W}{m*K}$ $h_{St.,fl.} = \frac{W}{m*K}$ $h_{St.,air} = \frac{W}{m*K}$

Table 4.1: Specific Parameter Values for the Geometry and Boundary Conditions.

4.5 Solution Methodology

Our methodology involves providing various input parameters for the 3D-printing operating state and the rheological characteristics of liquid chocolate and analyzing the outlet temperature in the form of a fluid temperature gradient in COMSOL. Heat Transfer and Fluid flow analysis is solved with a coupled analysis of the fluid flow and heat transfer on the inside of the nozzle to calculate outlet temperatures. Below is the specific model set-up methodology:

1) In "Geometry," an **axisymmetric** geometric model of the nozzle-chocolate interface is created in COMSOL in accordance with the dimensions and schematic provided above
2) A **fully-coupled physics solver** is selected, with"Steady-State Flow" and"Steady-State Heat Transfer" selected. Fluid flow and heat transfer boundary conditions are provided such as the conduction with the stainless steel nozzle, inlet temperature, inlet velocity, etc.

3) In “Materials,” custom material properties are provided for the fluid, including a function representation for the chocolate as a **Non-Newtonian fluid with the Cross-WLF Model**
4) A rectangular, sized mesh is computed with an “Extra-Fine” resolution and applied to the fluid and die, with variable cells (dependent on the outlet nozzle size)
5) Stationary results are computed in COMSOL for temperature, pressure, and velocity profiles
6) Complete **a parameter sweet for various nozzle lengths** (8 mm - 16 mm in 2 mm increments)
7) Complete **a parameter sweet for various nozzle diameters** (0.8 mm - 1.6 mm in 0.2 mm increments), and compile results into a sensitivity analysis plot to pinpoint the correct combination of geometry

5.0 RESULTS AND DISCUSSIONS

Thermal, velocity, and pressure analysis is conducted for various nozzle geometries through COMSOL finite-element method solver. After discretizing the predetermined geometry and optimization solver methods for our coupled analysis, various 2D line plots, 2D surface plots, and 3D diagrams are generated to describe the analytical outputs such as outlet temperature and maximum outlet velocity. Our team includes characterization plots for current nozzle geometries, in addition to other potential nozzles with different diameters and lengths. Finally, sensitivity analysis is computed to compare the sensitivity of the outlet temperature to determine the impact of nozzle diameter and length changes in optimizing the chocolate tempering temperature.

5.1 Mesh Convergence

In this study, the outlet temperature at the nozzle is the most important parameter. This location can be plotted with respect to temperature, so quantify the temperature difference. The mesh should allow for an accurate result at that location, and not change much if the mesh is further refined. Due to the sensitivity of temperature in such a small domain, a change of less than 0.01 K would signify that the model is not likely to change much with a finer mesh. The exit temperature can be seen as z = 0 on the left side of the plot. The origin of the geometry is at the bottom left corner of the fluid section, as it represents the axis of rotation for the axisymmetric behavior of the nozzle.

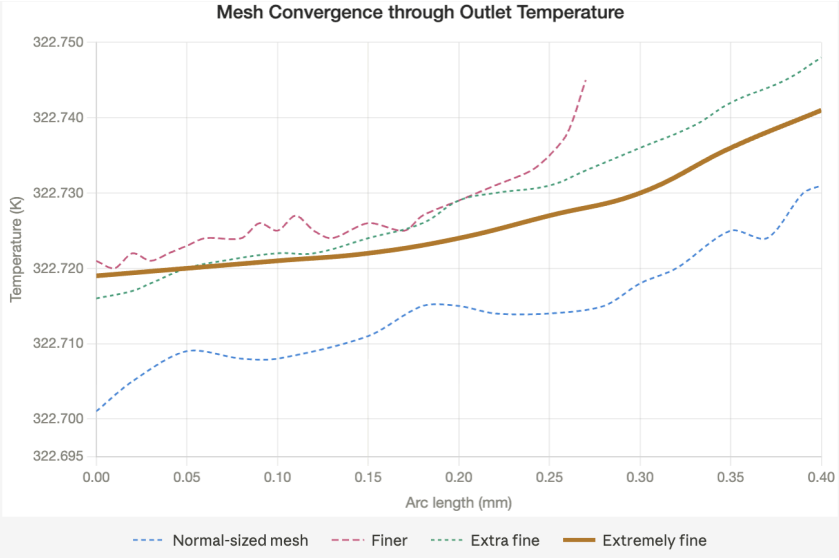

Figure 5.1: Overlaid Temperature over Outlet given by Mesh Refinement (“Normal,” “Finer,” “Extra Fine,” and “Extremely Fine”).

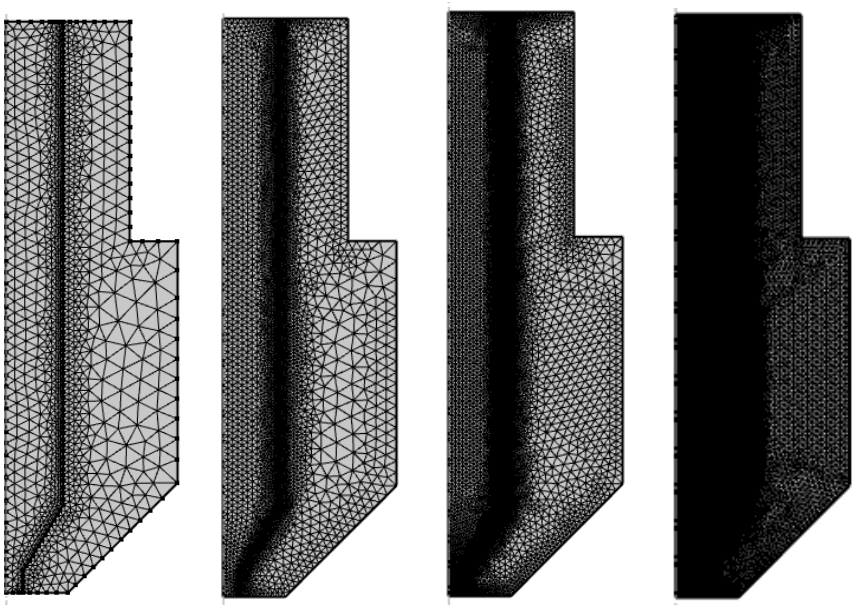

Figure 5.2: Normal, Fine, Extra Fine, and Extremely Fine Mesh Resolutions.

There is a significant amount of oscillation in the first three mesh curves, which demonstrates a not-converged mesh. After several mesh refinements, the solution converged to a point at which the exit temperature only changed by about 0.005 K. This validates that the model does not need further mesh refinement, which allows for a lower total computational load. The solution can now be deemed mesh-independent, where further meshing will not change the result in any significant manner (in this case, by any temperature difference lower than 0.005 K).

The final mesh, labeled “Extremely-Fine”, is more coarse on the outside of the steel wall, where little attention is paid to, as well as a slightly less coarse mesh on the inside of the fluid wall, at the axisymmetric boundary. A finer mesh is generated at positions of interest, such as the nozzle tip, and the fluid-wall interface. This is the location that requires the most precise results, so a mesh convergence is required to optimize the size with computational load. Further improvements to the mesh would include coarser elements on the die and around the inlet, while keeping the outlet fine, as only the outlet requires such small elements.

5.1.1 Current CocoaPress Velocity

As can be seen below, this coupled model outputs temperature, velocity, and pressure of the fluid and die. The velocity plot, in Figure 5.3, emphasizes that the fluid speeds up as it reaches the converging portion of the nozzle, which is the expected behavior in a nozzle of constant applied pressure. The

velocity increases by a factor of ~20x, from 0.025 m/s to 0.5 m/s. This value must be validated with known parameters (of known 3D print filaments) to see if such an increase is feasible. The velocity also increases radially towards the center of the flow, as seen in Figure 5.4.

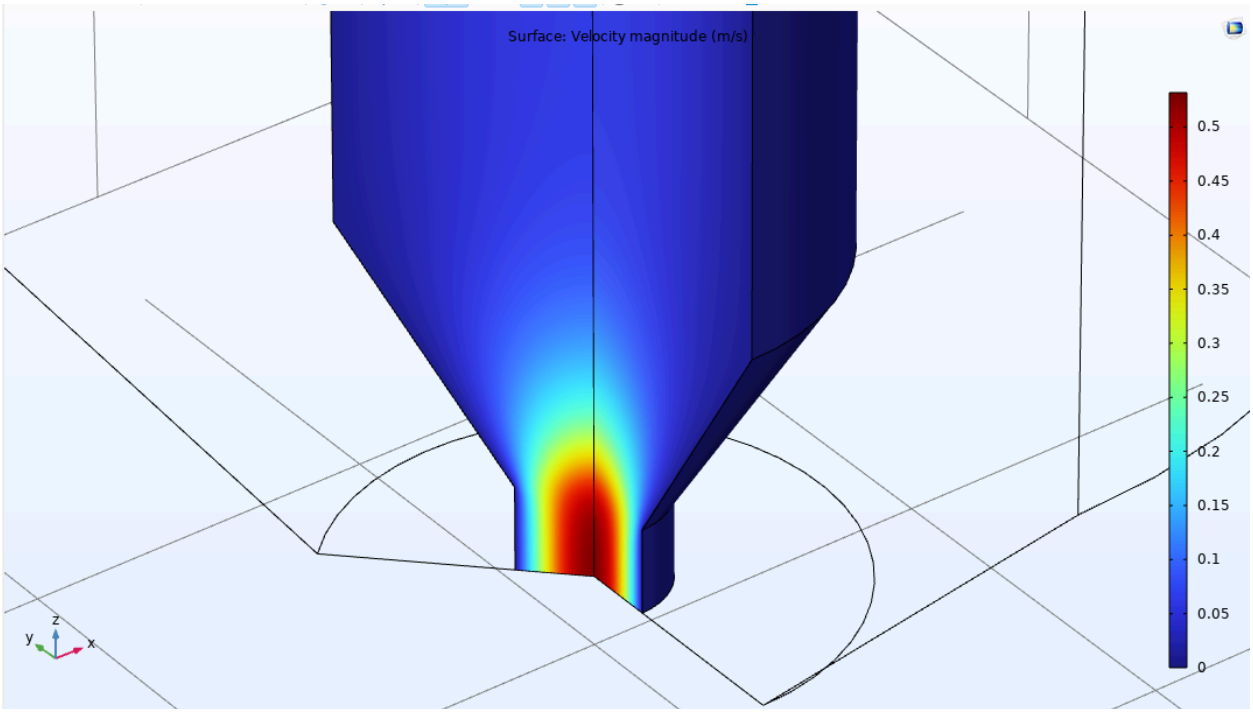

Figure 5.3: 3D Velocity Profile of Chocolate Flow Zoomed to Outlet.

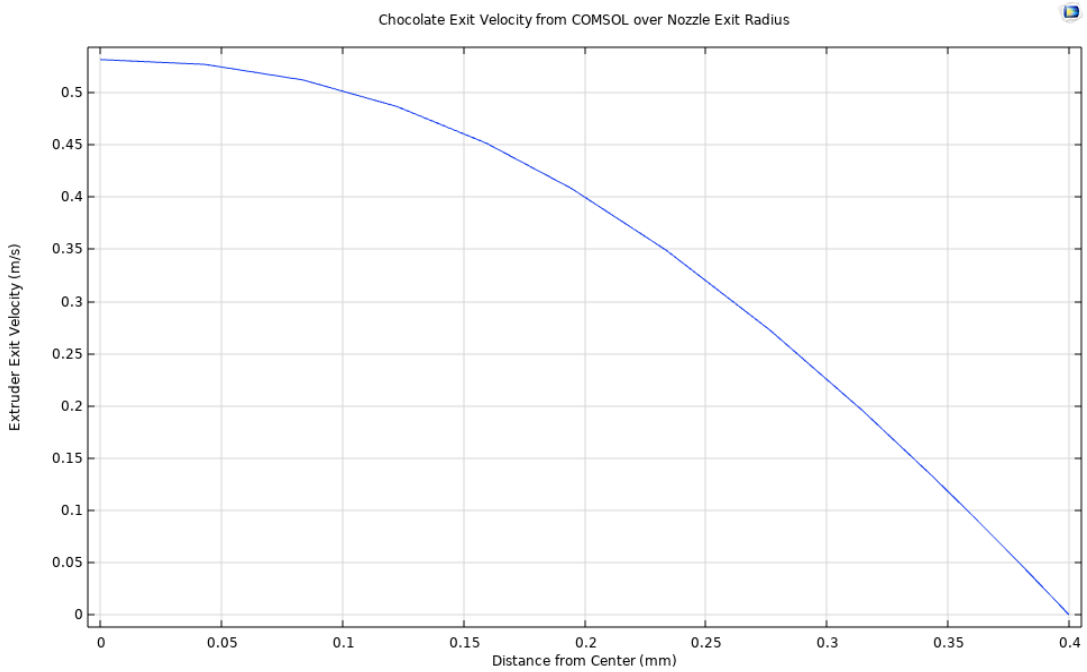

Figure 5.4: Velocity Across Nozzle Exit at Standard Nozzle Geometry and Flow Conditions.

5.1.2 Current CocoaPress Pressure

The pressure contours make sense in terms of usual FDM nozzle behavior. The pressure starts high in the chamber and decreases due to viscous losses along the wall as the fluid tracks downward. The pressure is lowest at the exit, which was set to atmospheric pressure as a boundary condition. Again, this result should be checked against known 3D print filament plastics, in order to validate, but initial results are promising.

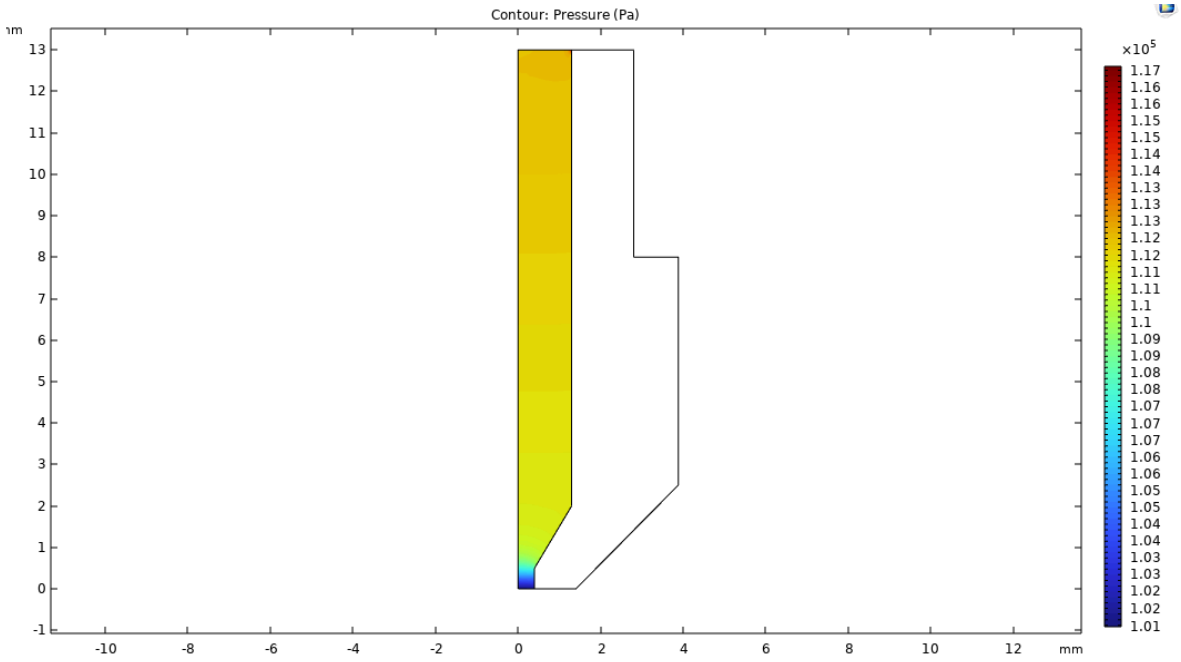

Figure 5.5: 2D Axisymmetric Contour Plot of Fluid Pressure.

5.1.3 Current CocoaPress Temperature

The temperature gradient is arguably the most important result. In order to prove, or disprove, the 3D printer's ability to temper chocolate, the exit temperature must be identified. The gradient behavior looks to be convincing in this plot, and behaves as one would expect. However, with a closer look at the key, while the temperature does change from 323 K to ~318 K, the majority of the surface area at the outlet is still at a higher temperature than desired. The output temperature of the chocolate should be around 306 K, which is the ideal tempering temperature. This may be because the CocoaPress does not temper their chocolate, and that this approximation is relatively accurate, or it could signify a problem with the model. The average temperature across the outlet, while lower than the axis point, is still relatively high, and does not significantly change the result.

It is also possible that the CocoaPress utilizes ambient temperature as the cooling mechanism, and cooling within the nozzle is not important. Chocolate does cool quickly under ambient conditions, so the CocoaPress could just rely on outside conditions to cool it, and the nozzle is used to control the output velocity and diameter.

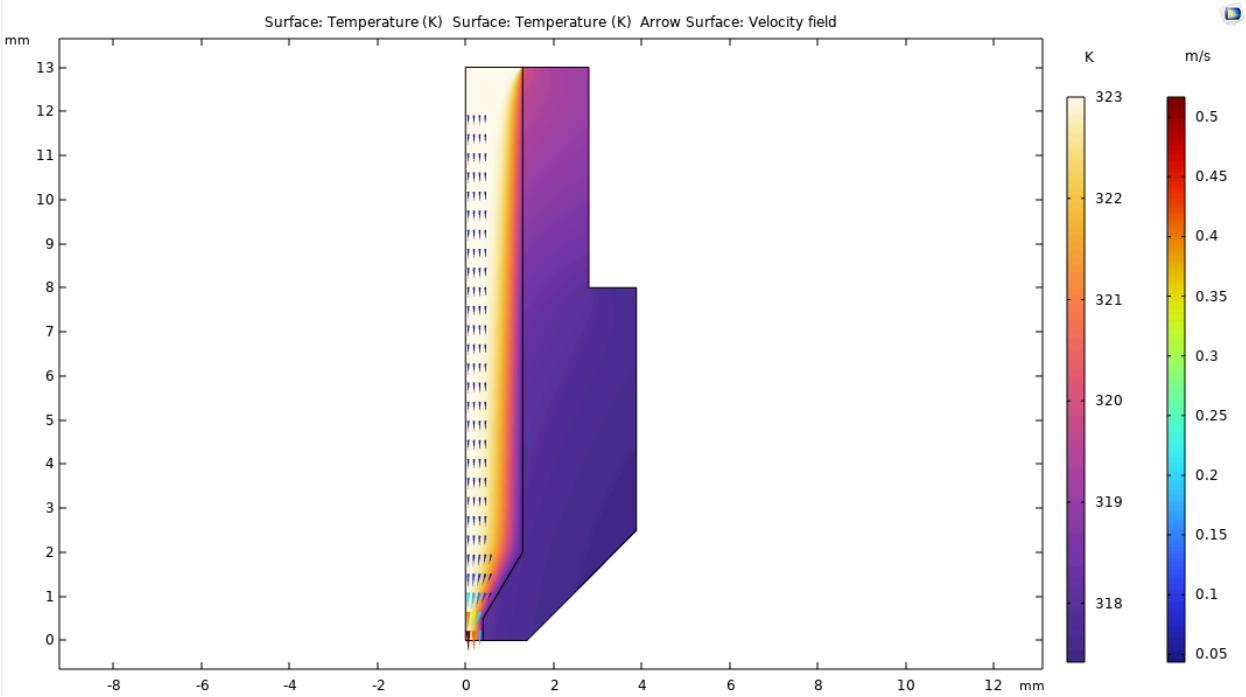

Figure 5.6: 2D Axisymmetric Plot of Temperature Gradient and Velocity Vectors.

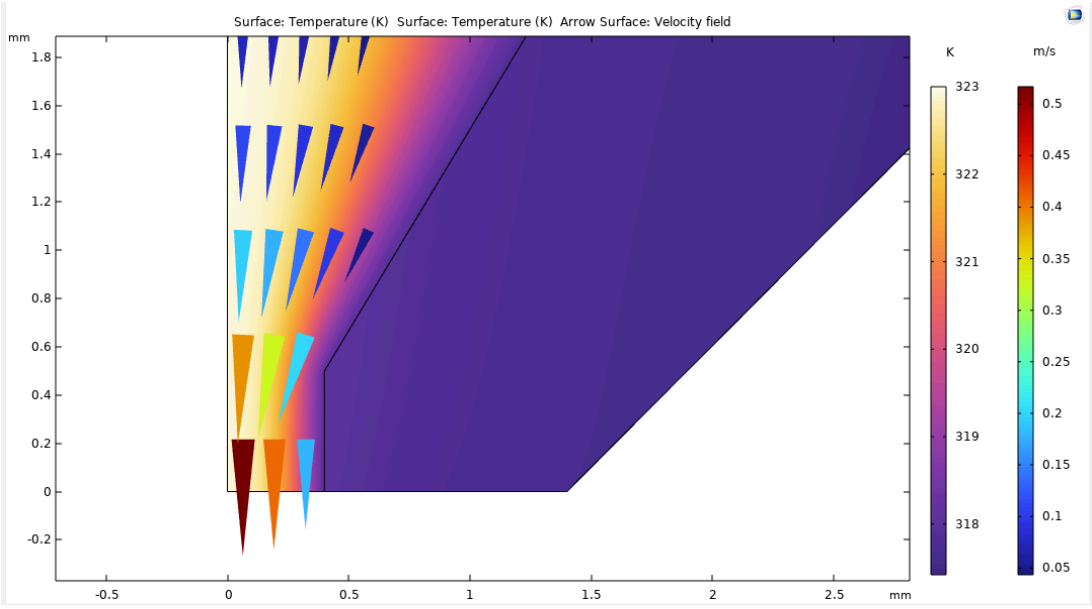

Figure 5.7: Enlarged Outlet showing Temperature and Velocity Gradients.

If it can be concluded that the temperature does not reach the ideal tempering conditions, adding cooling to the die boundary, at the top right, may be considered. This would cool the overall temperature along the length of the nozzle, allowing the chocolate to reach tempering conditions at the outlet, and perhaps have more uniformity along the radial direction.

5.1.4 Current CocoaPress Viscosity

In 3D printing, viscosity is an important parameter that gives insight as to how the fluid will behave as it is extruded. Proper, consistent viscosity is important to prevent clogging in the nozzle and ensure good inter-layer adhesion of a part.

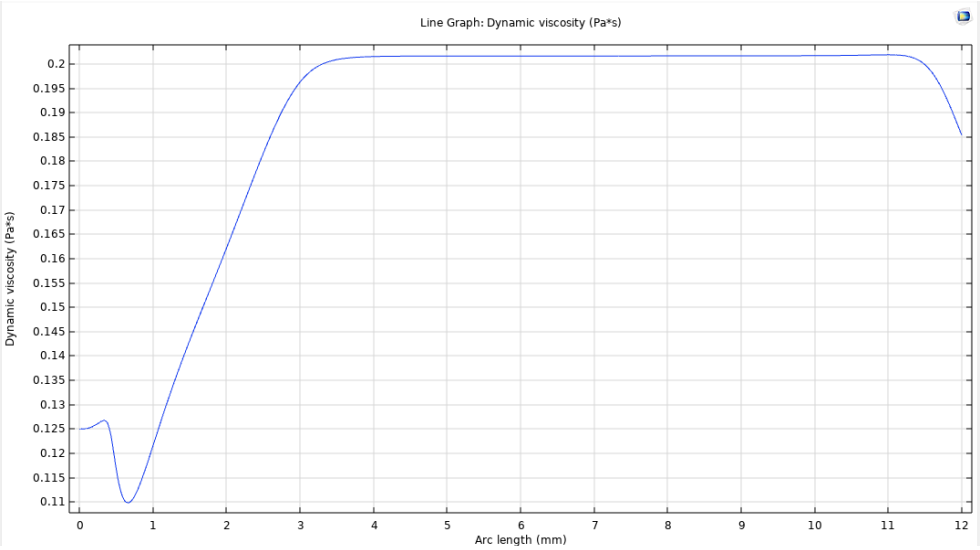

Figure 5.8: Chocolate Viscosity Magnitude in the Z-Direction Along Symmetric Axis with Z_{outlet} = 0 mm.

The Cross-WLF model of viscosity seems to be the correct approximation in this case. The equation for viscosity was implemented based on the parameters described in the appendix, and the shear rate was given by the internally calculated shear rate function, referenced as “spf.sr” in COMSOL. The viscosity decreases slowly towards the outlet, which is consistent with the PEEK plastic results that are discussed later in the paper. The viscosity has a sharp decrease around the converging section of the nozzle, which is consistent with viscosity being both temperature and pressure dependent. The Cross-WLF model was applied to PEEK plastic, as discussed in the next section, to ensure proper implementation of the equations. The equations are further described and derived in Appendix B.

5.2 Experimental Validation

To validate our model of the nozzle geometry for chocolate flow, we will use parameter substitution to check whether the model captures the correct physical behavior. By replacing the chocolate material properties with PEEK plastic material, given by Wang et. al [9], we can evaluate whether the governing physics and relationships will remain consistent. From the dependence of viscosity on temperature, to the effect of flow rate on pressure drop, and the role of heat transfer along the nozzle, we are able to analyze similarities between the two materials. The goal of this approach is not to match exact numerical values between materials, but to verify that the trends and physical relationships predicted by the model are correct. Current finite-element analysis models provide 2D contour maps of the fluid cross-section flowing through the nozzle, which serves as our primary comparison metric.

The PEEK parameters, given by the research paper, were then substituted into the original chocolate-based model so we could directly compare our results to those reported by other researchers (e.g., Wang et al.), providing a validation check for our modeling approach.

PEEK-Specific Parameters	PEEK-Specific Values
Critical shear (τ^*)	124,139 Pa
Empirical coefficient (A1)	36.041
Glass transition temperature (D2)	403.15 K
Inlet temperature (T_{In})	375 K
Inlet velocity (v_{in})	25.55 mm/s
Material density (ρ)	1.31 g/m^3
Power-law index (n)	0.4266
Specific heat (c_p)	1400 J/(kg·K)
Temperature-shift coefficient (A3)	51.6
Viscosity at ref. (D1)	2.9×10^{16} Pa·s

Table 5.1: PEEK Parameters from Wang et. al [9].

5.2.1 PEEK Velocity

Below are velocity magnitudes of PEEK fluid flow through a nozzle within our specific model infrastructure. Similar to previous results, the plot demonstrates acceleration at the convergence point, with a velocity range between 0.00 m/s and 0.88 m/s across the fluid area.

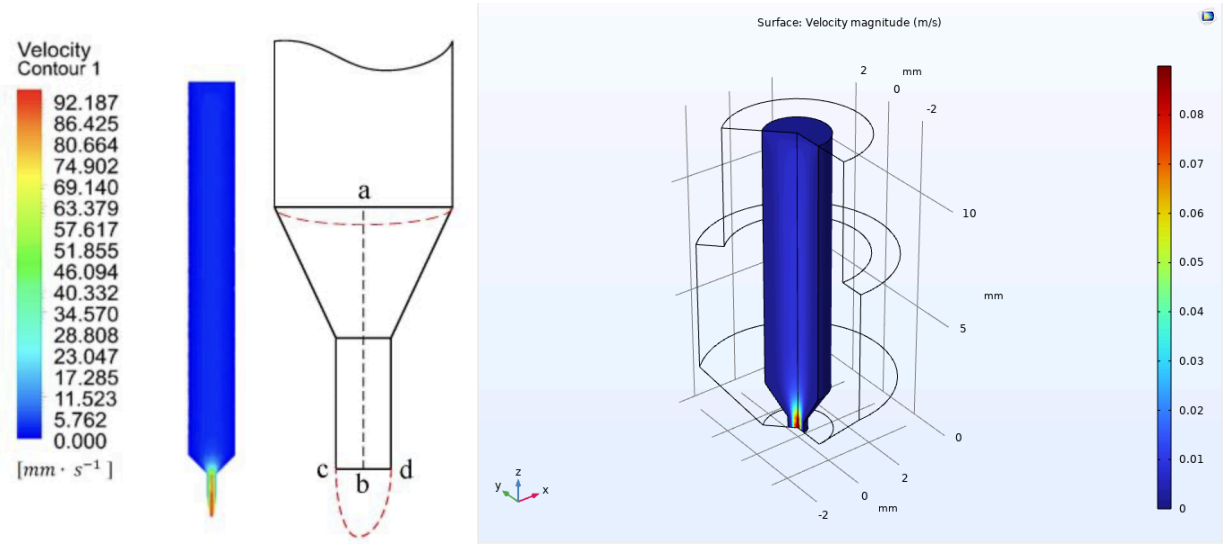

Figure 5.9: 3D Velocity Contour Plots for PEEK Filament of the research conducted by Wang et al. and by our specific model implementation.

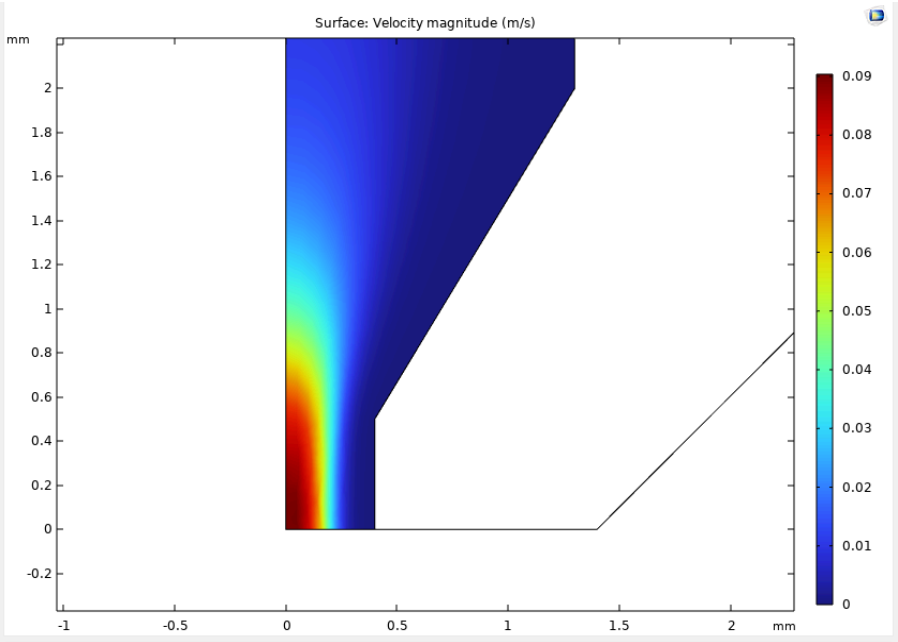

Figure 5.10: Zoom 2D Velocity Contour Plot for PEEK Filament.

Not only were the values very similar, but the model exhibited the same behavior. The researchers in this paper note “[t]he results showed that, as the nozzle diameter decreased, the melt pressure decreased, the speed increased, and the viscosity decreased” [9]. As can be seen from the velocity profile, and the viscosity plots of the chocolate, the behavior is the same. This is promising, and helps to validate that the developed solution represents the desired model. While this does not definitively prove an exact representation, this validation is a step in the right direction.

5.2.2 PEEK Temperature

The temperature gradients below in Figure 5.12 & 5.13 proves to be consistent both with the profiles seen with non-specific nozzle-based computations, and models provided by the Wang et al. research group. With temperatures between 375 K at the inlet to ~516.1 K at the outlet, the range is both realistic for PEEK material and consistent with the data provided. This is where our chocolate model differs from the PEEK model. The plastic model assumes that the material is heating up as it exits the nozzle, rather than cooling. This is represented here however, and proves that the model works for both heating and cooling-based approaches to 3D printing.

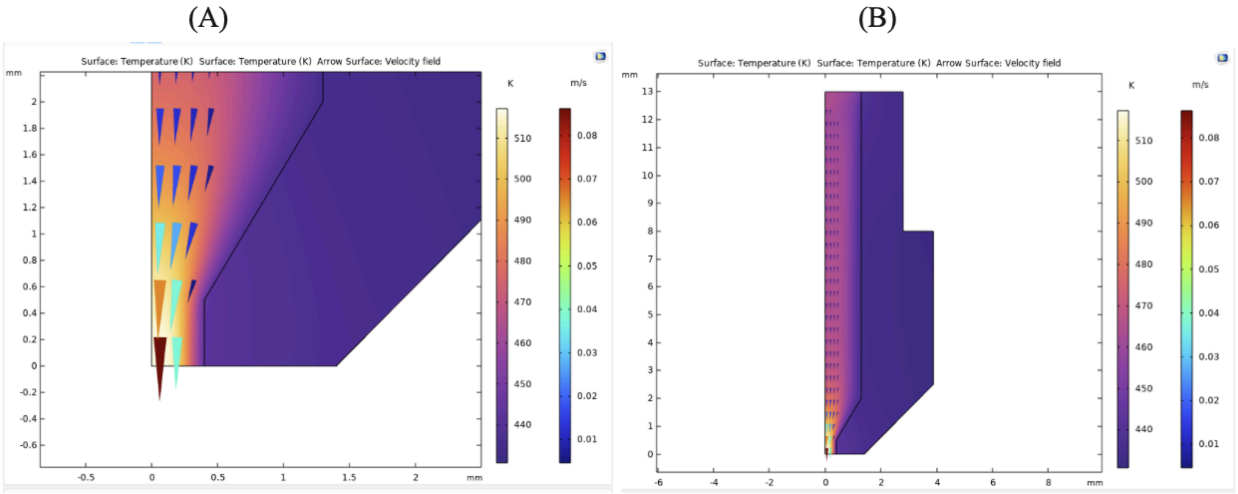

Figure 5.11: 2D Temperature Contour Plot for PEEK Filament (A) Zoomed; (B) Entire Surface.

5.2.3 PEEK Validation Conclusion

The velocity and temperature results from our PEEK-properties aligned well with the experimental trends reported by Wang et al. The simulated velocity peaked at ~0.088 m/s at the nozzle center and fell to 0 m/s at the walls, matching the bell-shaped profile shown in their extruder-exit data (~90 mm/s peak, 0 mm/s at edges). The model also produced a centerline temperature of ~516 K and an average outlet temperature of 482.44 K, which falls within the researchers’ reported range of 400–500 K.

Although the paper provides no specific temperature metric for direct error calculation, our results follow the qualitative behavior described.

5.3 Sensitivity Analysis

After validating the mathematical model, the next step is to run our sensitivity analysis on the geometric diameter and length of the nozzle. This will help us optimize the conventional nozzle designs for chocolate as a non-Newtonian fluid. Our group will primarily focus on these diameter and nozzle length parameters, as our initial intuition indicates these have the highest sensitivity relative to feed rate, inlet temperature, etc. Our research revealed outlet diameter is crucial towards temperature/velocity control and length is significant towards the overall cooling of the chocolate fluid.

For each case, key output metrics such as outlet temperature, velocity profile, shear rate distribution, and pressure drop, were measured. These outputs are critical because they directly influence print quality, structural integrity, and the risk of clogging or inconsistent flow. These insights allow us to recommend an optimized nozzle geometry and provide broader design guidelines for extrusion systems for non-Newtonian fluids like chocolate. While the current model we have does not suggest proper tempering, the sensitivity analysis, along with further geometry refinement, allows insight as to whether tempering can be achieved through geometry or if further cooling mechanisms, that have not been disclosed by the company, are required.

The sensitivity analysis was performed to quantify the effect of nozzle geometry on two key performance metrics: average outlet temperature and maximum velocity. These outputs were selected because they directly relate to extrusion quality, geometric dimensional stability, and the thermal behavior of the chocolate at deposition. Average outlet temperature is a good metric as to whether tempering is achieved within the nozzle, which is critical for controlling viscosity and ensuring consistent solidification at glass transition temperature after extrusion. Maximum velocity was used to capture peak flow within the nozzle, which is strongly influenced by geometric constructions and is directly related to shear-induced thinning effects in non-Newtonian fluids. Both nozzle diameter and length were systematically varied while maintaining constant inlet conditions to isolate geometric effects. The resulting trends in outlet temperature and maximum velocity were used to evaluate the coupled thermal–fluid response of the system and assess sensitivity of extrusion performance to nozzle design.

5.3.1 Temperature Sensitivity to Geometric Variation

Both nozzle length and diameter had a somewhat insignificant effect on outlet temperature, displayed in Figure 5.15. While this was not originally expected, this result actually has some value. The

variation in both length and diameter is not substantial enough at this scale to have a heavy influence on results. Nonetheless, there are minute changes to point out. Temperature consistently increases (however slight) as the diameter increases. This follows that a larger diameter increases the volume of fluid, which means more has to be cooled at the same temperature boundary, and therefore the fluid is more resistant to a temperature drop.

The length, however, did not seem to have a notable effect on temperature. In theory, shorter nozzles reduce time in the nozzle, leading to higher outlet temperatures and less thermal regulation, but it is assumed that the variability in the nozzle lengths tested is not enough to show a trend.

These results indicate that, under the current model assumptions, heat transfer is relatively insensitive to geometry changes compared to the imposed boundary conditions. In other words, the temperature gradient appears to be dominated by inlet temperature and wall conditions rather than nozzle length and outlet conditions. As a result, geometry alone does not significantly influence cooling or tempering potential in the current configuration.

(A) (B)

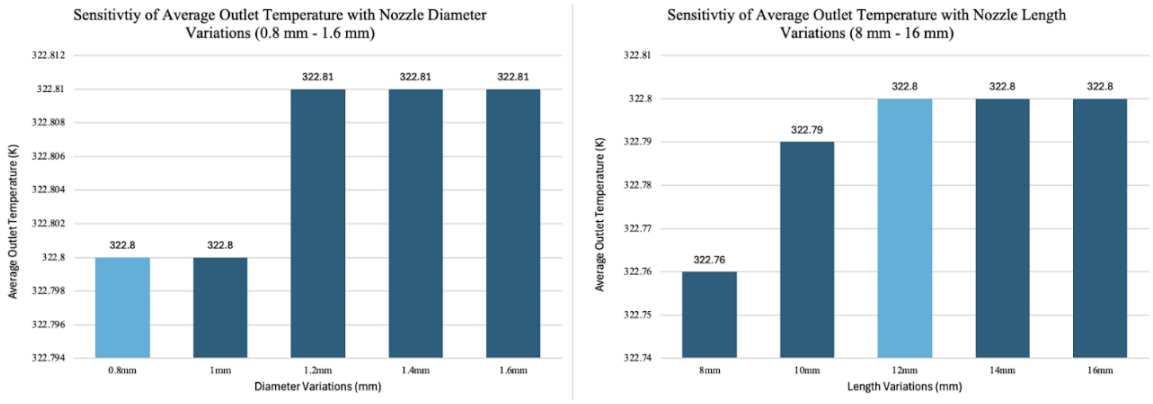

Figure 5.12: Changes in Average Outlet Temperature when (A) Diameter is Varied; (B) Length is Varied; with Baseline Highlighted in Light Blue.

5.3.1 Velocity Sensitivity to Geometric Variation

In contrast to temperature behavior, peak velocity, seen in Figure 5.16, showed a strong dependence on nozzle length and only a weak dependence on diameter. For all diameters, increasing nozzle length led to a consistent decrease in peak velocity. Shorter nozzles produced higher peak velocities, while longer nozzles resulted in lower and more stable velocity profiles.

This trend suggests that increasing nozzle length allows the flow to develop more fully and increases viscous resistance, which reduces peak flow acceleration. Beyond approximately 12–14 mm, the velocity begins to level off, indicating that the flow has reached a fully developed state and additional increases in length have little effect.

(A) (B)

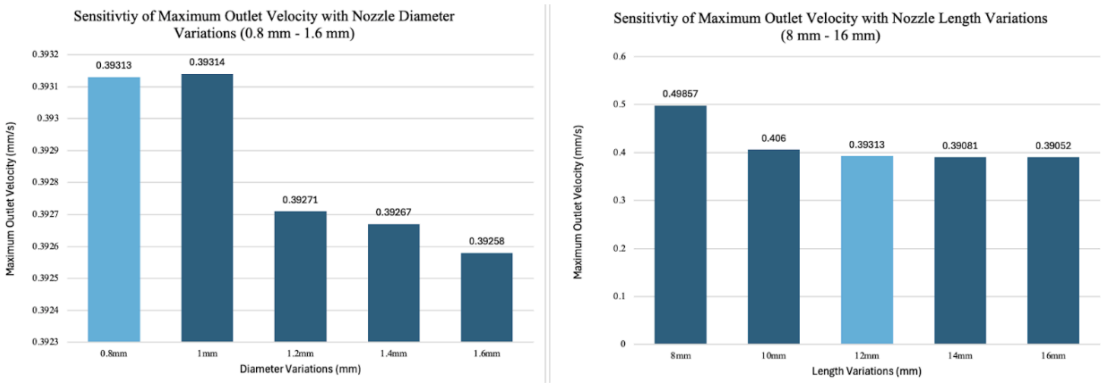

Figure 5.13: Changes in Peak Velocity when (A) Diameter is Varied; (B) Length is Varied; with Baseline Highlighted in Light Blue.

6.0 CONCLUSIONS AND DESIGN RECOMMENDATIONS

6.1 Conclusions

Based on our analysis, commercially available systems such as the Cocoa Press do not appear to temper chocolate during extrusion. Instead, we inferred that they rely on pre-conditioned or externally tempered chocolate prior to printing. This highlights a key limitation in the current design, where the nozzle primarily serves as an extrusion mechanism rather than a component capable of maintaining the correct temperature required for proper tempering. Even with optimized geometry, the nozzle has a minimal effect on temperature and flow conditions without additional thermal control strategies.

Given these limitations, further research is necessary to better understand the coupling between flow, heat transfer, and tempering behavior in chocolate extrusion. Future work would include exploring extended nozzle designs, active cooling or heating strategies, and alternative materials that may enhance temperature control. We plan to conduct experimental validation of our model by testing real printing conditions. This includes physically disassembling and analyzing a commercial Cocoa Press system to better understand its capabilities, as well as performing experiments to compare predicted and measured temperature profiles. These efforts will help determine whether the trends observed in our model hold in practice and guide the development of a more effective design for achieving tempering during chocolate 3D printing.

6.2 Design Recommendations

To improve the performance of chocolate 3D printers, one key recommendation is to focus on an optimal nozzle design that maintains a stable temperature profile from the reservoir to the outlet. The nozzle geometry should be designed to minimize heat loss while still allowing controlled cooling near the tip, which helps the chocolate transition into a semi-solid, structurally stable state after extrusion. This includes carefully selecting nozzle diameter, length, and material (e.g., stainless steel) to balance conduction and convection effects. A smaller outlet diameter may improve resolution and tempering consistency, but it must be balanced against increased pressure requirements and potential clogging. Overall, the optimal design should ensure that chocolate exits the nozzle within the desired tempering window, improving both structural strength and surface finish.

Another important consideration is design for manufacturability, particularly by leveraging axisymmetric geometries. Since the nozzle is rotationally symmetric, it can be efficiently manufactured using conventional processes such as CNC machining or lathe-based milling. This reduces production

cost, improves repeatability, and allows for tighter tolerances compared to more complex geometries. Simplifying the design to maintain axisymmetric also makes it easier to prototype and iterate quickly, which is especially valuable when testing multiple nozzle configurations. Additionally, smooth internal surfaces should be prioritized to reduce flow resistance and prevent material buildup, which can disrupt extrusion consistency.

Furthermore, ensuring compatibility across different chocolate 3D printer systems is critical for broader adoption and real-world application. The nozzle design should follow standardized interfaces so it can be easily integrated into commercially available printers like CocoaPress and similar platforms. Designing with modularity in mind allows users to swap nozzles based on desired resolution or material properties without modifying the entire system. This flexibility not only improves usability but also makes the design more scalable for different users, from hobbyists to commercial manufacturers. By combining optimized thermal performance, manufacturable geometry, and commercial modularity, the overall design can significantly enhance the effectiveness and practicality of chocolate 3D printing systems.

7.0 ORGANIZING THE END

7.1 Citations

[1] V. A. Fernandes, A. J. Müller, and A. J. Sandoval, “Thermal, structural and rheological characteristics of dark chocolate with different compositions,” *Journal of Food Engineering*, vol. 116, no. 1, pp. 97–108, May 2013, doi: https://doi.org/10.1016/j.jfoodeng.2012.12.002.

[2] “Cocoa Press 2.0 Professional Package – 3D Chocolate Printer Fully Assembled,” *Cocoa Press*, https://cocoapress.com/products/cocoa-press-2-pro-3d-chocolate-printer-fully-assembled (accessed Feb. 12, 2026).

[3] S. T. Beckett, M. S. Fowler, and G. R. Ziegler, “Useful Physical Constants,” *The Manufacturing Confectioner*, pp. 667–668, Dec. 2008, doi: https://doi.org/10.1002/9781444301588.oth1.

[4] Engineers Edge, “Specific Heat Capacity of Metals Table Chart,” *Engineersedge.com*, Jan. 11, 2015. https://www.engineersedge.com/materials/specific_heat_capacity_of_metals_13259.htm

[5] L. Zhou and S. Su, “Design and Validation of a Piston-Driven Syringe-Extrusion Bioprinter Using an FDM Frame,” *Biomimetics*, vol. 10, no. 12, p. 811, Dec. 2025, doi: https://doi.org/10.3390/biomimetics10120811.

[6] “Stainless Steel - Specific Heat and Thermal Conductivities vs. Temperatures,” *www.engineeringtoolbox.com*. https://www.engineeringtoolbox.com/stainless-steel-specific-heat-thermal-conductivity-vs-temperature-d_2225.html

[7] H. Banks, “The Density of Chocolate A student project by Harriet Banks,” 2012. Available: https://www.density.co.uk/documents/Density-of-Chocolate.pdf

[8] G. Whitaker, “What Temperature Does Chocolate Melt At?,” *Whitakers Chocolates UK*, 2026. https://www.whitakerschocolates.com/blogs/blog/what-temperature-does-chocolate-melt-at?srsltid=AfmBOoqctEZM9tUFpy2Ky8jI_XoYvuA1PJttuOmRm-ZuibzgGCoBNzME (accessed Apr. 24, 2026).

[9] J. Wang, H. Hu, Z. Liu, Y. Shi, and Y. Huang, “Optimization of 3D Printing Nozzle Parameters and the Optimal Combination of 3D Printer Process Parameters for Engineering Plastics with High Melting Points and Large Thermal Expansion Coefficients,” *Materials*, vol. 18, no. 3, p. 500, 2025, doi: https://doi.org/10.3390/ma18030500.

[10] E. Edge, “Grashof Number (GR),” *Engineersedge.com*, 2026. https://www.engineersedge.com/heat_transfer/grashof_number_gr_15781.htm (accessed Apr. 24, 2026).

[11] “UCSB Science Line,” *Ucsb.edu*, 2020. http://scienceline.ucsb.edu/getkey.php?key=7019

[12] Editor Engineeringtoolbox, “Air Viscosity: Dynamic and Kinematic Viscosity at Various Temperatures and Pressures,” *Engineeringtoolbox.com*, Jan. 25, 2003. https://www.engineeringtoolbox.com/air-absolute-kinematic-viscosity-d_601.html?vA=298&units=K#

[13] “Rheology Model Fitting and Corrections,” *blog.rheosense.com*. https://blog.rheosense.com/rheology-model-fitting-and-corrections

[14] X. Gao, T. Guo, F. Han, Y. Tian, and Z. Zhang, “Rheological and Sensory Properties of Four Kinds of Dark Chocolates,” *American Journal of Analytical Chemistry*, vol. 06, no. 13, pp. 1010–1018, 2015, doi: https://doi.org/10.4236/ajac.2015.613096.

[15] C. Press, “What Can You Print? - Cocoa Press Documentation,” *Cocoapress.com*, 2026. https://help.cocoapress.com/Advanced/PrintableDesigns/#maximum-volume (accessed Apr. 24, 2026).

7.2 Appendix

Appendix A - Calculating Convection Constant, h, for Forced Air Over Nozzle

$Gr = gL^3 \xi \Delta T / v^2$ [10]

$g = gravity$ (9.8 m/s^2)

$L = length\ of\ surface$ (13mm)

$\xi = coefficient\ of\ expansion\ of\ the\ fluid$ (3.4 x 10^{-3}/deg K) [11]

$\Delta T = surface\ temp\ vs\ fluid\ temp$ (let's assume 15 degK)

$\nu = kinematic\ viscosity\ of\ the\ fluid$ (15.51e-6 m^2/s)

$Gr = (9.8\ m/s^2)(0.013\ m)^3(.00341/K)(15\ K)/(15.51e-6\ m^2/s)^2$

$Gr = 4569$

Nusselt Number: $Nu = C(Gr * Pr)^n$

Prandtl Number: $Pr = \frac{\mu C_p}{k}$

$\mu = dynamic\ viscosity$ (18.36e-6 Pa*s) [12]

$C_p = 1012\ J/kg * K$

$k = 0.025\ W/mK$

$Pr = \frac{(18.36e-6)(1012)}{0.025} = 0.743$

For laminar cylinder: $Nu = 0.59(Gr * Pr)^{1/4}$

$Nu = 0.59(4569 * 0.743)^{1/4}$

$Nu = 4.5$

$h = \frac{Nu \cdot k}{L} = 4.5(0.025)/0.013$

$h = 8.65\ W/m^2K$

Appendix B - Cross Model and Williams-Landel-Ferry Model for Temperature-Based Viscosity

Temperature-Dependent Viscosity Model (Cross Model): $\eta = \frac{\eta_0}{1+(\frac{\eta_0 * \dot{\gamma}}{\tau^*})^{1-n}}$ [13]

Zero-Shear Viscosity Model (WLF Model): $\eta_0 = D_1 * exp(\frac{-A_1(T-D_1)}{A_3+(T-D_2)})$

Cross-WLF Constants of Generic 70% Dark Chocolate [14]					
Critical Shear Stress [Pa]	**Power-Law Index**	**Viscosity at Reference Temp. [K]**	**Glass Transition Temp. [K]**	**Empirical Coefficient**	**Temp.-Shift Coefficient**
τ^*	n	D_1	D_2	A_1	A_3

168	0.6226	6	298.15	10	51.6

Cross-WLF Constants of Generic 70% Dark Chocolate Viscosity vs. Shear Reconstruction[14]		
Viscosity (u)	**Shear (T)**	**Linear Comp.**
Pa*s	**s^-1**	**s^-1**
26.5	4	6.0224
16	8	5.9648
12.5	12	5.9072
10	16	5.8496
8.5	20	5.792
6.5	24	5.7344
6	28	5.6768
5.75	32	5.6192
5.5	36	5.5616
5.25	40	5.504
5	60	5.216
4	150	3.92
Fitting Equation		y = -88.8*x+504

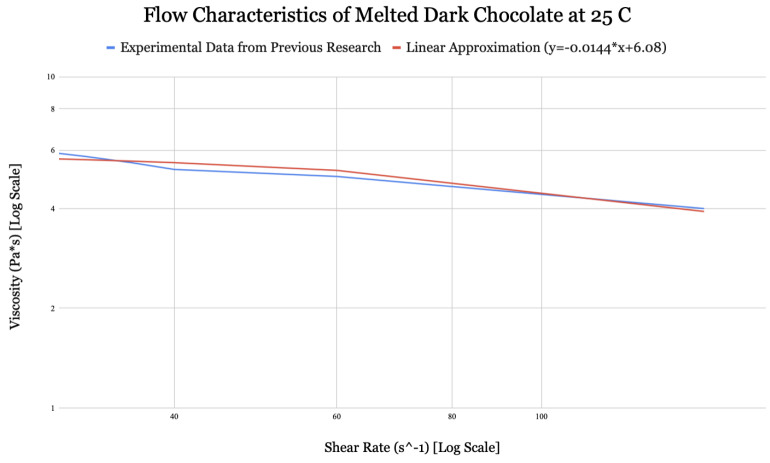

Figure 7.1: Reconstruction of the Experimental Data from Previous Research against the specific fitting function chosen to determine relevant Cross-WLF constants

Approximation of Temperature-Dependent Viscosity with the Applicable Cross-WLF Constants					
Critical Shear Stress [Pa]	**Power-Law Index**	**Viscosity at Reference Temp. [K]**	**Glass Transition Temp. [K]**	**Empirical Coefficient**	**Temp.-Shift Coefficient**
τ^*	n	D_1	D_2	A_1	A_3
168	0.6226	6	298.15	10	51.6

Final Representation for Viscosity Terms

$$\eta = \frac{\eta_0}{1+(\frac{\eta_0 \dot{\gamma}}{168})^{1-0.6226}}$$

$$\eta_0 = 26.5 * exp(\frac{-10(T-298.15)}{51.6+(T-298.15)})$$

Appendix C - Estimating Feed Rate

The CocoaPress website has a slicer settings troubleshooting page where a sample slicer output panel is given. This panel includes total time to print as well as total volume of chocolate used. From here, an estimate for feed rate is calculated using these parameters with nozzle diameter.

$$Volume = 72,367.34\, mm^3$$

$$Time = 26\, min * 60\, \frac{sec}{min} = 1560\, sec$$

$$Nozzle\ Area = \pi r^2 = \pi(0.8mm)^2 = 2.011mm^2 \text{ (assuming larger diameter nozzle)}$$

$$Feed\ Rate = \frac{Volume}{Time*Area} = \frac{72{,}367.34\, mm^3}{1560\, s * 2.011mm^2} = 23.07\, \frac{mm}{s}$$

If this estimated printing time includes ramp up time, it can be assumed that the feed rate is a little bit larger than the 23.07 mm/s value. A conservative estimate of around 25 mm/s was used in this model for simplicity.

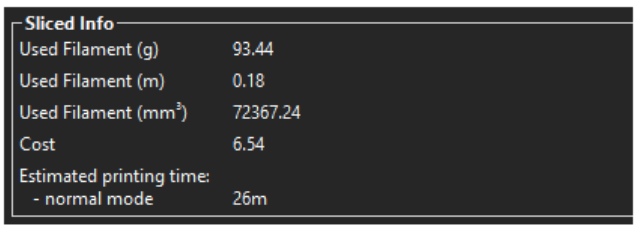

Figure 7.2: CocoaPress Slicer Output Panel [15]